Strategizing well locations in unconfined, heterogeneous hydrate reservoirs for maximizing gas production

Neelam Choudhary [a], Jyoti Phirani [b],*

[a] Department of Chemical Engineering, Indian Institute of Technology Delhi, Hauz Khas, Delhi 110016, India
[b] Department of Civil and Environmental Engineering, University of Strathclyde, Glasgow, G1 1XJ, UK

ARTICLE INFO

ABSTRACT

Natural gas hydrates are a potential alternative to conventional energy due to their high energy density and low carbon with wide distribution across the globe. Producing methane from the gas hydrate reservoirs is technically challenging as they are present in complex geological environments which are highly heterogeneous. In this work, using numerical reservoir simulations of gas production from oceanic gas-hydrate reservoirs underlain with an aquifer we show that warm-water injection is necessary when the water layer below the hydrates is unconfined. Our simulations reveal that the aquifer characterization is essential to design the gas production strategy and estimating the gas recovery. We demonstrate that for a gas-hydrate reservoir attached to a moderately unconfined aquifer, warm-water injection in the hydrate-zone leads to more recovery. If the hydrate-zone is layered then the gas recovery improves by injecting the water into a more porous layer. However, for highly unconfined reservoirs water should be injected near the aquifer for efficient recovery of gas. Our findings will help in developing gas production plans from the hydrate reservoirs around the world.

1. Introduction

Fossil fuels will be a significant part of the energy mix in the net-zero scenario (Liu and Li, 2021). However, the quest for cleaner replacement of conventional energy sources has increased. Natural gas is the most clean burning fuel compared to conventional energy sources (Kakaee and Paykani, 2013). Hence, natural gas can become the potential replacement for oil and coal. Natural gas is present in the large volume in the gas hydrate reservoirs in nature. The abundance of methane hydrates found in geological reservoirs, approximately $10^{18} m^3$, makes it an attractive energy resource to explore intensively as a possible alternative to conventional energy resources (Li et al., 2021; Reagan et al., 2015; Milkov, 2004; Kvenvolden, 1999). The methane hydrates are distributed in deep oceanic water sediments and in permafrost, which provides conducive temperature–pressure conditions for hydrate formation and stability (Reagan et al., 2015; Wan et al., 2020; Sloan, 1998). Hydrates may spontaneously dissociate due to climate change and lead to methane release, therefore, it is important to explore them as an energy resource (Matsumoto, 2002; Hesselbo et al., 2000). However, producing methane from this solid crystalline clathrate structure of gas and water molecules, which is stable at high pressure and low temperature, requires technology and thorough knowledge of the reservoir complexities (Bhatnagar et al., 2006; Kvenvolden, 1993). The effectiveness of the methane production technology used is governed by how it controls the heat and mass transfer and hence the temporal and spatial advances of methane hydrate dissociation in the reservoir. The dissociation of methane hydrates into methane and water molecules is an endothermic process, therefore, the fluid flow and heat transfer process needs to be thoroughly examined to produce methane from these unconventional deposits (Sloan, 1998; Yamamoto et al., 2019; Konno et al., 2010; Moridis et al., 2007).

The decrystallization equation of methane hydrates into water and gas can be written as;

$$CH_4 \cdot nH_2O(h) \rightleftharpoons CH_4(g) + nH_2O(w), \qquad (1)$$
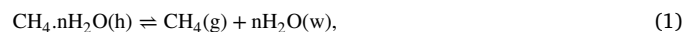
where, the ratio of water to gas molecules in a hydrate molecule, represented by n, is the hydration number for hydrates (around 6 for methane hydrates). The destabilization of methane hydrate can be achieved by introducing external disturbances in the reservoirs. The equilibrium curve of pressure and temperature (P–T curve) for methane hydrates as illustrated in Fig. 1 (Sloan, 1998) gives us the destabilization conditions. In the diagram, the presence of an aqueous phase can be seen above the temperature of 273.15 K and the ice phase below the temperature of 273.15 K. The hydrate is stable above the G-A-H equilibrium curve and the gas phase is stable below this curve. The quadruple point has conditions for all four phases to coexist.

---

* Corresponding author.
  E-mail address: jyoti.phirani@strath.ac.uk (J. Phirani).

Nomenclature

λ	Effective thermal conductivity W/m/K	
μ_j	Viscosity of fluid phase j	
ϕ	Porosity	
ϕ^e	Effective porosity of fluid phases	
ϕ_o	Reference porosity	
ρ_j	Density of phase j Kg/m^3	
ρ_R	Rock density Kg/m^3	
ρ_R	Sand internal energy J/Kg	
F^i	Flux of component i	
g	Gravitational force	
H_j	Specific heat of phase j J/Kg	
J_j^i	Molecular diffusion of component i in phase j	
K	Absolute permeability mD	
k_o	Reference permeability mD	
K_{rj}^o	End point relative permeability mD	
n_j	Exponential parameter of phase j	
P_{ce}	Entry capillary pressure MPa	
P_c	Capillary pressure MPa	
P_j	Pressure of phase j	
q	Source or sink term	
S_{jr}^e	Residual saturation	
S_j	Saturation of phase j	
S_j^{e*}	Normalized saturation of phase j	
U_j	Internal energy of phase j J/m^3	
v_j	Velocity of phase j	
W_j^i	The Weight fraction of component i in phase j	
k_{rj}	Phase relative permeability	
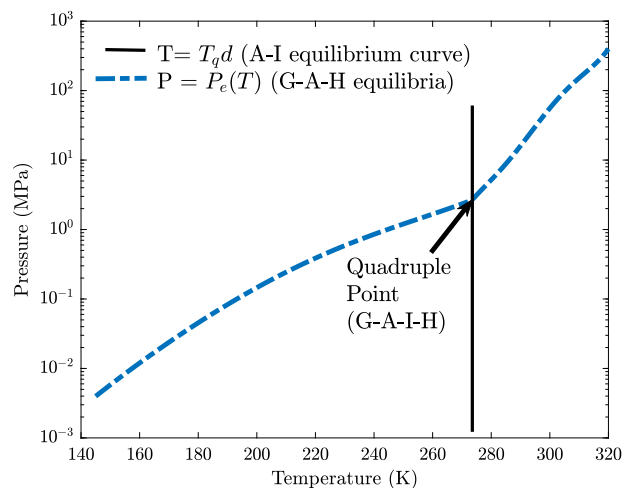
Fig. 1. Sloan's P–T curve for methane hydrates (Sloan, 1998; Choudhary and Phirani, 2022).

According to the Pressure–Temperature equilibrium curve (P–T curve) (Sloan, 1998) of methane hydrates as shown in Fig. 1, four basic techniques can be used to destabilize the methane hydrate and produce methane from these unconventional methane deposits; depressurization, thermal stimulation, inhibitor injection and CO_2 injection. In the depressurization method (Zhao et al., 2015; Bhade and Phirani, 2015b; Uddin et al., 2014; Phirani and Mohanty, 2009), the reservoir pressure is decreased from the initial pressure and the sensible heat of sediments is used to dissociate hydrates. In the thermal stimulation method (Bhade and Phirani, 2015a; Li et al., 2016; Phirani et al., 2009a,a), the temperature of the reservoir is raised above the initial reservoir temperature either by steam injection or by warm water injection to destabilize the methane hydrate. In the inhibitor injection method (Li et al., 2017; Kamath et al., 1987; Makogon et al., 1997; Sira et al., 1990), the chemical inhibitors like salt or alcohol which inhibit the formation of hydrates by shifting the current equilibrium phase curve upwards, are injected. In the CO_2 injection method (Mohebbi and Behbahani, 2014; Phirani et al., 2010; Graue et al., 2006), methane molecules in hydrate crystals are displaced by injecting compressed CO_2 molecules which results in simultaneous methane production and CO_2 sequestration. Four classifications of hydrate deposits are identified based on the underburden and overburden layer (Makogon, 2010; Milkov and Sassen, 2001), which are; Class-1 deposits, where a free gas layer is present below the hydrate layer; Class-2 deposits, where the hydrate layer is underlain by an aquifer layer; Class 3 deposits, where hydrate layer is present between shale layers; Class-4 deposits are low saturation hydrate deposits in dispersed form.

The first short-term offshore production test in 2013, in Eastern Nankai Trough, Japan presented the possibility of gas production from the offshore gas hydrate reservoirs. However, the gas produced during the entire period was 119000 m^3 and lasted for a few days (Yamamoto et al., 2019; Matsuzawa et al., 2014; Yamamoto et al., 2014). This was due to the complexities of gas hydrate reservoirs at the bottom of the ocean, which need to be analysed further and require accurate predictions through numerical simulations. In 2017, Japan conducted its second offshore production test at Eastern Nankai Trough which lasted for 36 days (Yamamoto et al., 2019). In the same year, another offshore production test was conducted in the South China Sea, China (Hao et al., 2017). These successful production tests represent the feasibility of gas production at a larger scale given the reservoir complexities are well understood and studied to successfully produce methane gas (Agency for Natural Resources and Energy (ANRE) and Japan Oil, Gas and Metals National Corporation (JOGMEC), 2017; Myshakin et al., 2012; Yamamoto et al., 2017). Therefore, numerical simulations are used to understand the fluid flow and transport behaviour in the reservoir and to predict the potential complexities during gas recovery from gas hydrate reservoirs for a long duration.

A large volume of gas is present in the K–G basin site NGHP-02-09 as gas hydrates, which have a large aquifer underneath it. Simulations suggest that the presence of the aquifer reduces the ability to depressurize the reservoir to recover the gas (Boswell et al., 2019). It is important to understand the field development plan using simulations for these class-2 reservoirs which will depend on the hydraulic connectivity between the hydrate zone and the aquifer below along with properties of the hydrate bearing sediments and aquifer properties. In the literature, we see that the heterogeneity of the reservoir has a significant impact on the reservoir behaviour due to the coupled heat and mass transfer, and hydrate dissociation phenomena (Wan et al., 2020; Boswell et al., 2019; Dai et al., 2012; Luo et al., 2015). Feng et al. (2019) suggested a strong effect of the permeability of layers on gas recovery from multilayered gas hydrate reservoirs. Yuan et al. (2017, 2018) studied flow behaviour in layered gas hydrate reservoirs and suggested that the dissociation of hydrate was significantly impacted by the layering of the reservoir. However, strategies of well placement for a field development plan for efficient production dependent on the reservoir properties are underreported. For class-2 hydrate reservoirs, it also becomes important to study the effect of the aquifer properties on gas production. In this work, we highlight the importance of aquifer characterization in developing production strategies for unconfined class 2 hydrate reservoirs. We use simulations to investigate how layering in the hydrate zone and unconfinement in the aquifer zone affect gas production efficiency. We find that the unconfinement of the aquifer plays a significant role in determining the heat transfer mechanism in the hydrate reservoir, which subsequently impacts the optimal well placement strategy for
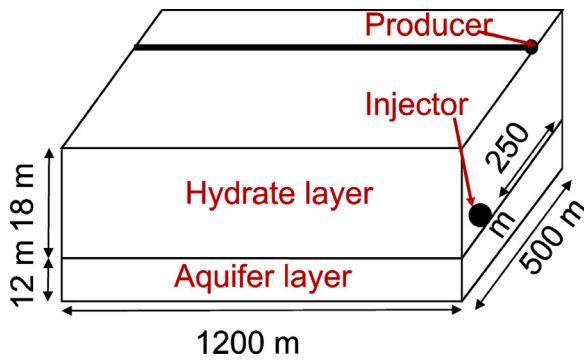
Fig. 2. Unconfined reservoir block and well placements considered in the model.

Table 1

Thermodynamic properties considered in the model in line with the K–G basin NGHP-02-09(Jang et al., 2019; Kida et al., 2019).

1	Initial reservoir porosity (ϕ)	0.42
2	Initial hydrate layer Permeability (k_1)	0.31 mD
3	Saturation of hydrate (S_h) in hydrate layer,	0.75
4	Saturation of water (S_w) in hydrate layer	0.25
5	Aquifer layer water saturation (S_w)	1
6	Initial Permeability of sand without hydrates (k)	1803 mD
7	Initial reservoir pressure (at the bottom)	31.458 MPa
8	Pressure at injection well	50 MPa
9	Initial reservoir temperature (at the bottom)	294.88 K
10	Temperature at injection well	323.15 k
11	Pressure at production well (k_0)	4 MPa

maximizing gas production and reducing water production. This study emphasizes the need for a comprehensive understanding of the aquifer's characteristics to develop effective production strategies for unconfined class 2 hydrate reservoirs.

2. Reservoir model and methodology

An unconfined reservoir block, which is thermodynamically similar to the Krishna–Godavary basin in India at site NGHP-02-09, located around 300 m below the seafloor (Collett et al., 2019), is considered. The initial temperature at the bottom of the reservoirs is 294.88K and the initial pressure at the bottom of the reservoir is 31.458 MPa. The initial reservoir temperature and pressure vary with the reservoir depth by a geothermal gradient of 0.03^0 C/m and hydrostatic gradient, respectively. The reservoir dimensions are shown in Fig. 2 which is 1200 m long and 500 m wide with a thickness of 30 m. An infinite aquifer layer of 12 m thickness is considered below a hydrate layer (18 m). An infinite aquifer is simulated by considering the permeability 1/10th of the initial reservoir permeability for the bottom 3 m layer of the aquifer. The under-burden layer is assumed to have a constant pressure boundary condition and water flow is permitted between the under-burden and bottom grid layer according to the pressure difference. The mass transfer is restricted at the overburden, however, heat transfer is permitted at both over-burden and under-burden with a coefficient of heat transfer. The lateral boundaries are assumed to be in symmetry, therefore, no mass or heat transfer is considered through the lateral boundaries. The reservoir domain is discretized into 25 × 12 × 10 grid blocks. The remaining reservoir properties are given in Table 1. Both the warm water injection and depressurization methods are used to explore an unconfined gas hydrate reservoir. One horizontal warm water injector is placed in the aquifer layer and one horizontal producer at the top, located 250 m apart, as shown in Fig. 2. Different well locations are studied which are mentioned in the following sections.

2.1. Numerical models applied in the simulator

The simulator which has been used in this work is a 3-D finite volume, multi-phase (accounts for aqueous, gas, hydrate and ice), multi-component (accounts for water and methane) simulator, developed by Sun and Mohanty (2006). The formation and dissociation of hydrate in the simulator are assumed in the equilibrium because of the relatively fast kinetics of gas hydrate dissociation (Kim et al., 1987). The governing nonlinear energy and mass balance partial differential equations (PDEs) are discretized in the time and space domain obtaining nonlinear algebraic equations. The Finite volume method is incorporated to obtain spatial discretization which is further discretized in time by the backward Euler method to give a fully implicit scheme of solution. These equations are further solved by the Newton–Raphson method. The phase transition is captured by changing the primary variables at different time steps using the primary variable switch method

(PVSM) (Falta et al., 1992). The simulator has been validated against other available simulators worldwide in the US DOE code comparison study and history matched with experimental evaluation of hydrate formation and dissociation (Wilder et al., 2008; Phirani et al., 2009b).

The governing equations for energy and mass balance are described below,

Equation of mass balance

$$\frac{\partial}{\partial t}\left(\phi \sum_{j=G,A,H,I} \rho_j S_j W_j^i\right) + \nabla \cdot \overline{F}^i = q^i, \tag{2}$$

Equation of energy balance

$$\frac{\partial}{\partial t}\left(\phi \sum_{j=G,A,H,I} (\rho_j S_j U_j) + (1-\phi)(\rho_R U_R)\right) + \nabla \cdot \overline{F}^e = -q^e, \tag{3}$$

where porosity is represented by ϕ, the density of phase j (gas, aqueous) by ρ_j, the saturation of phase j by S_j and weight fraction of component i in phase j by W_j^i, the combined internal energy by U_j, the flux of component i by F^i, and the source or sink term by q. The fluid flow in porous media determines the convective flux based on the flow properties and is given by multi-phase Darcy's law.

In Eq. (2), flux for convection and dispersion is given as

$$F^i = \rho_G v_G W_G^i + \rho_A v_A W_A^i + J_G^i + J_A^i, \tag{4}$$

where velocity is represented by v_j and the molecular diffusion of component i in phase j by J_j^i. In Eq. (3), the energy flux by convection and conduction is given as

$$F^e = \rho_G v_G H_G^i + \rho_A v_A H_A^i - \lambda \nabla T, \tag{5}$$

where the specific heat is represented by H_j^i and the effective thermal conductivity by λ. The phase velocity by multi-phase Darcy's law is given as

$$\overline{v_j} = -K\left(\frac{k_{rj}}{\mu_j}\right) \cdot \left(\nabla P_j + \rho_j \overline{g}\right), \tag{6}$$

where Darcy's velocity is represented by $\overline{v_j}$, the absolute permeability by K, viscosity by μ_j, the relative permeability by k_{rj}, pressure for phase j by P_j and the gravitational force by $\overline{g}$.

2.2. Transport models used in the simulator

The effective permeability in the porous media is described by the Power law model (Civan, 2001; Civan et al., 2002b,a), as given by the equation,

$$\frac{K}{K_o} = \frac{\phi^e}{\phi_0}\left[\frac{\phi^e(1-\phi_0)}{\phi_0(1-\phi^e)}\right]^{2\beta} \tag{7}$$

where, ϕ^e represents the effective porosity available for fluid phases (gas and aqueous) during hydrate formation and dissociation which may vary due to the dynamic nature of the hydrates. At the reference porosity ϕ_o, K_o is the reference permeability and β is assumed to be 2. The effective porosity ϕ^e is given by the equation,

$$\phi^e = \phi(S_G + S_A), \tag{8}$$

(a) Overall gas recovery (% OGIP) from homogeneous reservoir block at different reservoir porosity

(b) Ratio of gas by water (GWR) of homogeneous reservoir block at different reservoir porosity
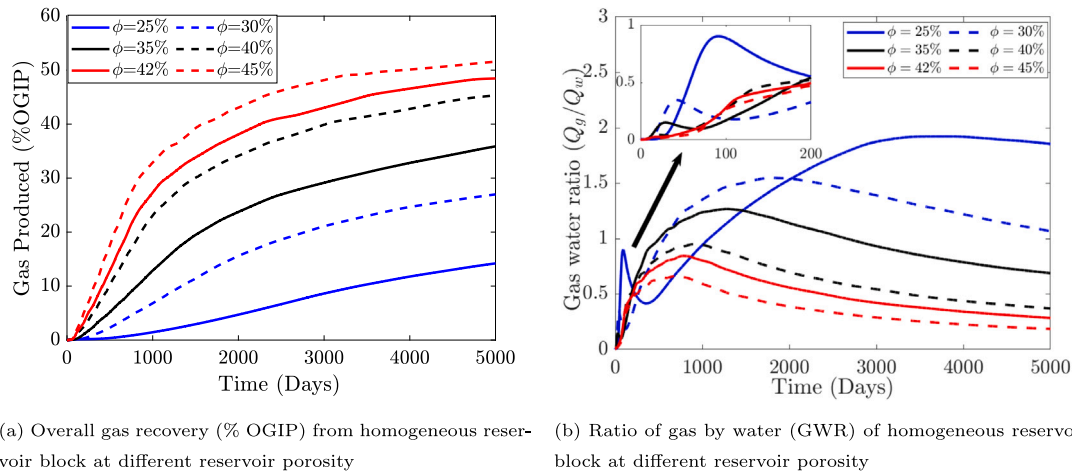
Fig. 3. Overall gas recovery (% OGIP) and the ratio of Gas by water at different reservoir porosity for homogeneous reservoir.

Table 2
Thermodynamic constants considered in the simulator.

1	Ice density	917.1 kg/m^3
2	Hydrate density	910 kg/m^3
3	sand density	2670 kg/m^3
4	Residual aqueous saturation	0.2
5	Residual gas saturation	0.0
6	Hydrate heat capacity	1.62 kJ/kg/K
7	Sand heat capacity	0.83 kJ/kg/K
8	Reference Permeability (k_0)	100 md
9	Reference Porosity (ϕ_0)	0.28
10	Permeability Rock Constant (β)	2
11	Sand heat conductivity	5.57 W/m/K
12	Gas Relative Permeability exponent (n_G)	2
13	Pore Structure Parameter (n_c)	5
14	Water Relative Permeability exponent (n_w)	4
15	Hydrate heat conductivity	0.49 W/m/K

where, absolute porosity is represented by ϕ, the saturation of the aqueous phase by S_A and the saturation of gas by S_G. The relative permeability and capillary pressure in the model are calculated by the Brooks–Corey model, Brooks and Corey (1964) as given below

$$K_{rG} = K_{rG}^o (S_G^{e*})^{nG}, \tag{9}$$

$$K_{rA} = K_{rA}^o (S_A^{e*})^{nA}, \tag{10}$$

$$P_c = P_{ce}(S_A^{e*})^{-nc}, \tag{11}$$

where, the endpoint relative permeability is represented by K_{rj}^o and n_j is an exponential parameter of phase j. Capillary pressure is represented by P_c and the capillary pressure at entry by P_{ce}. S_j^{e*} represents the normalized saturation of phase j, given by the equation below,

$$S_j^{e*} = \frac{S_j^e - S_{jr}^e}{1 - S_{Gr}^e - S_{Ar}^e}, \tag{12}$$

where, S_j^e is the fluid phase saturation. The residual saturation S_{Gr}^e for the gas phase is considered to be 0 and 0.2 for the aqueous phase residual saturation S_{Gr}^e. Other constants are listed in Table 2 and the rest of the details about the simulator can be found in Sun and Mohanty (2006).

2.3. Investigation methodology

To investigate the impact of layers on gas production, firstly the response of different sediment porosity on gas recovery in a homogeneous gas hydrate reservoir was analysed. The Civan's power law model (Civan, 2001; Civan et al., 2002b,a) used in the simulator states that low porosity sediments have low permeability, however, the total

gas hydrates in the reservoir also are less, requiring low dissociation energy if we consider the same saturation in the reservoir. Therefore, investigating the effect of porosity will inform us of the dominant process at different reservoir porosity. However, the reservoir considered in this work is not isolated and is attached to an unconfined aquifer, therefore the effect of aquifer properties on the gas production potential of the reservoir was also examined. Next, this work introduces layers in the hydrate bearing sediments and evaluate the production for different layering patterns and suggest well locations for efficient production for different scenarios.

3. Results and discussion

3.1. Effect of porosity in homogeneous unconfined reservoir

In this study, the reservoirs of different porosity were considered as described in Section 2 and assumed everything else remains unchanged. The producer and the injector locations are shown in Fig. 2. A pressure of 4 MPa is maintained at the producer. At this depressurization pressure, we do not see ice formation as seen in previous studies which apply depressurization pressure lower than the quadruple point of the hydrate phase diagram (Aminnaji et al., 2017). The warm water is injected at a pressure of 50 MPa and a temperature of 323.15K. The porosity governs the permeability of the hydrate and the aquifer zones, therefore low porosity means lower unconfinement of the aquifer, low permeability of the sediments and less hydrates present in the reservoir at the same hydrate saturation. Fig. 3(a) shows the gas produced for reservoirs of different porosity. We see that the percent gas recovery is higher for the reservoir with high reservoir porosity. The saturation profiles of hydrate shown in Fig. 4 also show that high reservoir porosity leads to hydrate dissociation in the larger volume of the reservoir. Fig. 3(b) shows the gas water ratio (GWR) to understand the water handling required for gas production. Higher porosity leads to higher injectivity of the warm water and lower aquifer confinement, therefore a lower gas water ratio for high porosity reservoirs is observed. However, when the porosity is 25% the gas water ratio shows a different behaviour for initial periods as can be seen in Fig. 3(b). This behaviour can be seen in all the cases till about 100 days as shown in the inset of Fig. 3(b). This is because initially the water production is less due to the low mobility of water in comparison to the gas in the hydrate bearing zone. Once the water from the unconfined aquifer reaches the producer we see a decrease in the GWR. Then, due to the low confinement of the aquifer in the high porosity reservoirs, the water production is high and as the gas production rate decreases between 1000 to 2000 days (Fig. 3(a)) then we see the gas water ratio decreasing. However, in the low porosity reservoir, the water production is less as compared to the

(a) Hydrate saturation profile for homogeneous reservoir at 25% porosity

(b) Hydrate saturation profile for homogeneous reservoir at 30% porosity

(c) Hydrate saturation profile for homogeneous reservoir at 35% porosity

(d) Hydrate saturation profile for homogeneous reservoir at 40% porosity

(e) Hydrate saturation profile for homogeneous reservoir at 42% porosity

(f) Hydrate saturation profile for homogeneous reservoir at 45% porosity

Fig. 4. Hydrate saturation profiles at $5000 days$ of homogeneous reservoir block at different reservoir porosity.

(a) Overall gas recovery (% OGIP) at different aquifer porosity

(b) Ratio pf gas by water at different aquifer porosity
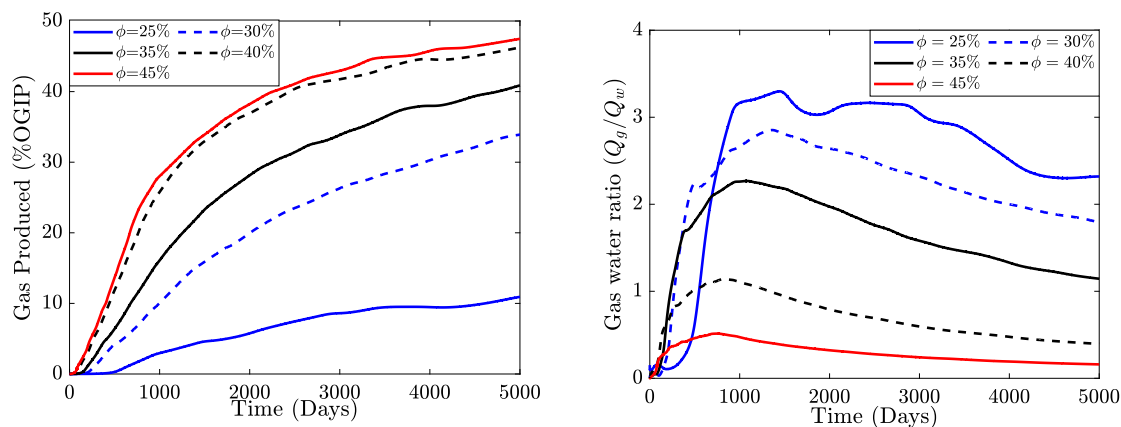
Fig. 5. Overall gas recovery (% OGIP) and the ratio of gas by water at different aquifer porosity.

gas production due to higher confinement of the aquifer layer which leads to the increased gas water ratio.

As a whole, the results indicate that the aquifer size and confinement that is governed by the porosity of the aquifer have a large effect on the gas recovery from the gas hydrate reservoir. This can be concluded because the permeability of the hydrate bearing zone is less due to the presence of the hydrates and hence, the aquifer permeability has the major contribution to the reservoir behaviour. Further, this study specifically explore the effect of the aquifer layer and its confinement on gas production from the gas hydrate reservoirs.

3.2. Effect of aquifer layer and its confinement

The aquifer size and confinement are governed by the porosity of the aquifer. The aquifer also governs the warm water injection into the

reservoir (Choudhary and Phirani, 2022). Therefore, this work considers the reservoir described in Section 2, injector and producer locations as in Fig. 2. The injection and production conditions are as in the section above. Now, this study examines the gas production potential of the reservoirs that are attached to different porosity aquifers. The porosity of the hydrate layer is considered 42% which is constant for all the cases. Different cases are studied where the aquifer has a porosity between 25% and 45% and observed the percent gas recovery and gas water ratio from the reservoir as shown in Fig. 5. It can be seen that the percent gas recovery decreases from 47% to 11% comparing the case when aquifer porosity is 45% to the case when aquifer porosity is 25%. This decrease is comparable to what we see in Fig. 3(a). The hydrate saturation profiles at the end of the simulation are also comparable as seen in Figs. 4 and 6. Therefore, the gas recovery potential of an unconfined class-2 reservoir is largely dependent on the aquifer size
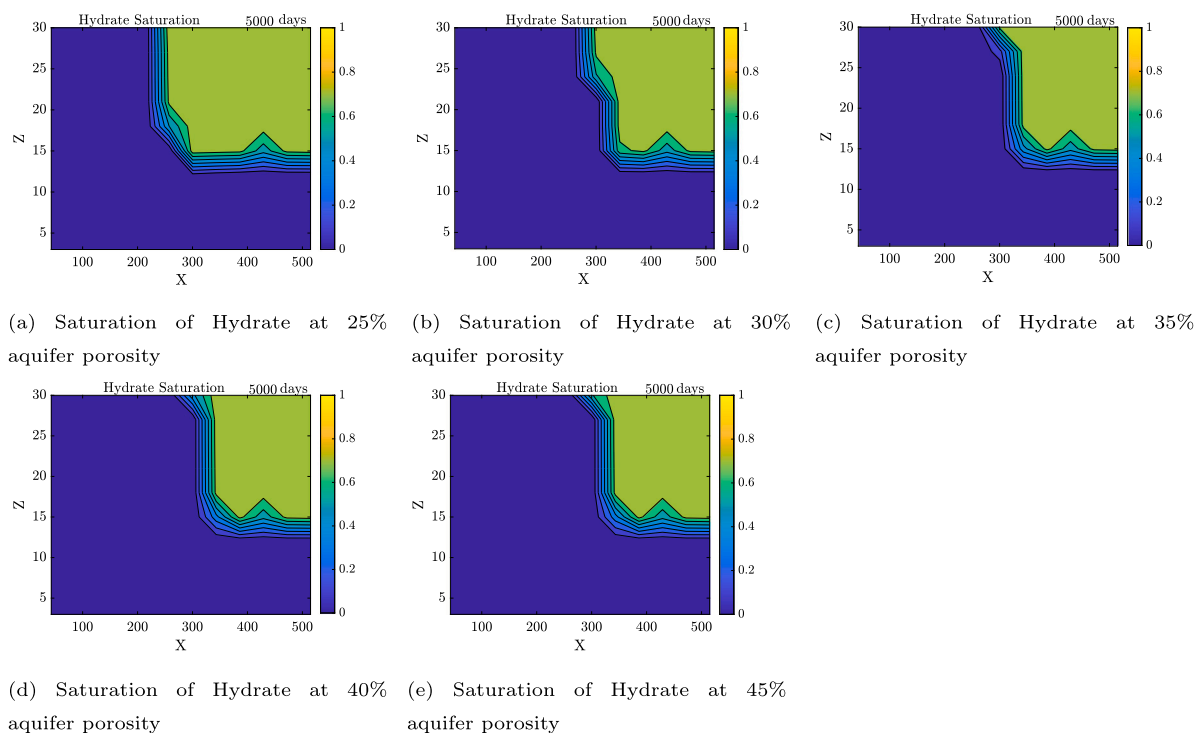
(a) Saturation of Hydrate at 25% aquifer porosity

(b) Saturation of Hydrate at 30% aquifer porosity

(c) Saturation of Hydrate at 35% aquifer porosity

(d) Saturation of Hydrate at 40% aquifer porosity

(e) Saturation of Hydrate at 45% aquifer porosity

Fig. 6. Hydrate saturation profiles at $5000 days$ at various aquifer porosity and constant hydrate layer porosity of 42%.

(a) Overall gas recovery ($\%OGIP$) at different aquifer porosity when horizontal injector is at middle of hydrate layer

(b) Overall gas recovery at (% OGIP) different aquifer porosity when horizontal injector is at top of hydrate layer
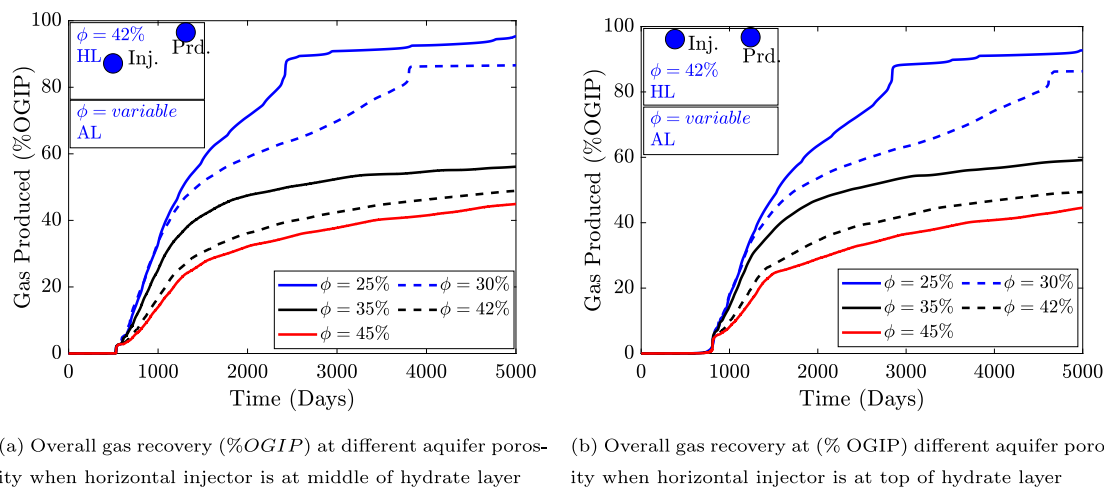
Fig. 7. Gas recovery profiles (% OGIP) for different well placements in the hydrate layer.

and confinement governed by the aquifer porosity. This is because the gas recovery in these kinds of reservoirs is governed by warm water injection. The convection of the warm water is facilitated by the aquifer and hence the mobility of water in the aquifer changes the potential production. The gas water ratio in Fig. 5(b) is also comparable to the gas water ratio shown in Fig. 3(b).

3.3. Effect of injector location in unconfined reservoirs

At the low porosity of the aquifer, the aquifer is becoming less unconfined. Therefore, the study explores the effect of injector location on the production potential of these hydrate reservoirs. Fig. 7 shows the percent gas recovery for two different injector locations shown in the inset of the figures. In Fig. 7(a), the injector is 9 m below the top of the hydrate bearing zone. In Fig. 7(b), the injector is at the top of the hydrate bearing zone. We observe that the overall gas recovery

does not change significantly for the highly unconfined aquifer by changing the injector location comparing the results in Figs. 5(a) and 7(a). The injector location in the hydrate zone delays the start of gas production as predicted by Choudhary and Phirani (2022). However, for the aquifers which are less unconfined and have low porosity, the injector in the hydrate zone and away from the aquifer increases the gas production potential 6–8 times in comparison to the case when the injector was near the aquifer as shown in Fig. 5. Hydrate saturation profiles in Fig. 9 and Fig. 10 also show significant hydrate dissociation in the reservoir with the injector in the hydrate zone. This is because of the low permeability of the aquifer the injected water preferentially flows in the high permeability hydrate zone dissociating the hydrates. For 25% and 30% aquifer porosity cases, we see a sudden increase in gas production before the gas production plateaus. This is because, all the hydrates between the injector and producer have been dissociated by that time, which increases the water flow and helps dissociate hydrates on the right in the proximity of the producer (see insets of
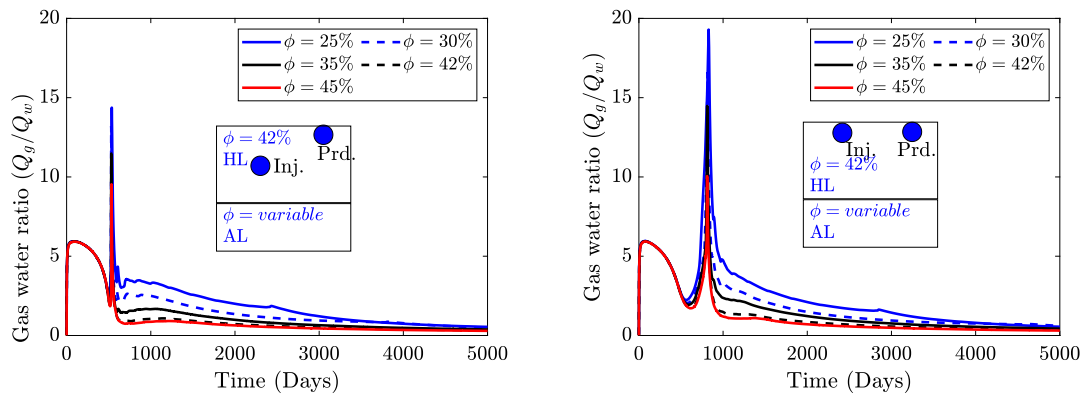
(a) Ratio of gas by water at different aquifer porosity when horizontal injector is at middle of hydrate layer

(b) Ratio of gas by water at different aquifer porosity when horizontal injector is at top of hydrate layer

Fig. 8. Ratio of gas by water for different well placements in the hydrate layer.
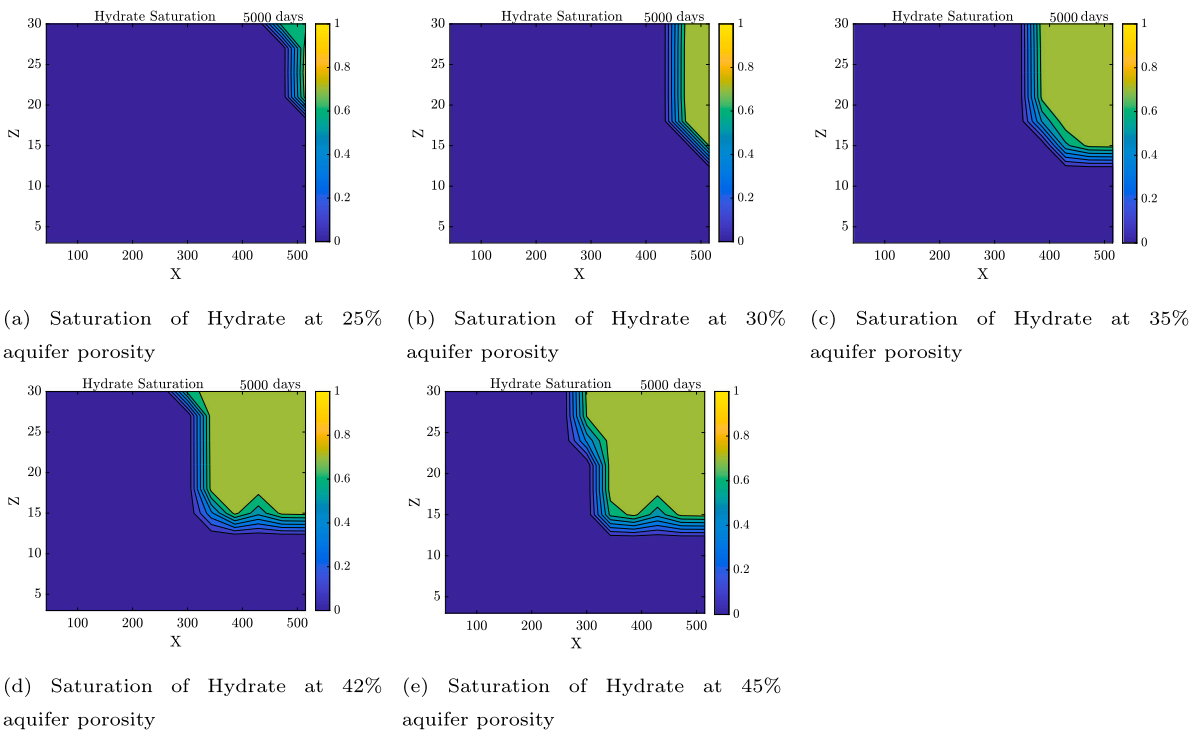
(a) Saturation of Hydrate at 25% aquifer porosity

(b) Saturation of Hydrate at 30% aquifer porosity

(c) Saturation of Hydrate at 35% aquifer porosity

(d) Saturation of Hydrate at 42% aquifer porosity

(e) Saturation of Hydrate at 45% aquifer porosity

Fig. 9. Hydrate saturation profiles at $5000 days$ at various aquifer porosity and constant hydrate layer porosity of 42% when injector is at the middle of hydrate layer.

Figs. 7, and 9 and 10). The total gas and water production till about 500 days is insignificant and a peak in the gas water ratio is seen in Fig. 8 when the gas production starts. Before the start of gas production, the gas water ratio is inconsequential for practical purposes and the water production has the same order of magnitude as gas production afterwards.

3.4. Effect of layers in the hydrate zone

We see from the above analysis that if the aquifer is large and highly unconfined then we can dissociate about 50% of hydrates by injecting warm water near the aquifer. However, if the aquifer is moderately unconfined then we can dissociate approximately 85% of the hydrates by injecting warm water in the hydrate zone. This work now introduces layers in the hydrate zone and observe the impact of these layers on gas recovery. Different aquifer confinements are considered and used 45% and 30% aquifer porosity for these cases. These aquifer porosities

lead to different gas production behaviours for homogeneous hydrate zone as seen in Fig. 7 and therefore they are considered for further investigation of the layered hydrate zone. For both low and high aquifer porosity, two hydrate layers are considered, hydrate layer 1 (HL1) and hydrate layer 2 (HL2) as shown in the insets of Fig. 11. The average porosity of the hydrate layer is considered as 42% for all the cases. Along with the layers, the injector and producer well location are also investigated. The different well locations investigated are shown in Table 3. Three different injector locations are investigated; near the aquifer, at the interface of HL1 and HL2 (9 m below from the top) and at the top of the hydrate layer. The producer in these three cases is located at the top of the hydrate layer. Further, to investigate the impact of producer location on the gas recovery, the producer in the middle of the hydrate layer is also considered for all these cases. The percent gas recovery for all the cases is shown in Fig. 11. We see from Fig. 11(a) that the location of the warm water injector has a large effect on the overall production and the production rate.

(a) Saturation of Hydrate at 25% aquifer porosity

(b) Saturation of Hydrate at 30% aquifer porosity

(c) Saturation of Hydrate at 35% aquifer porosity

(d) Saturation of Hydrate at 42% aquifer porosity

(e) Saturation of hydrate at 45% aquifer porosity
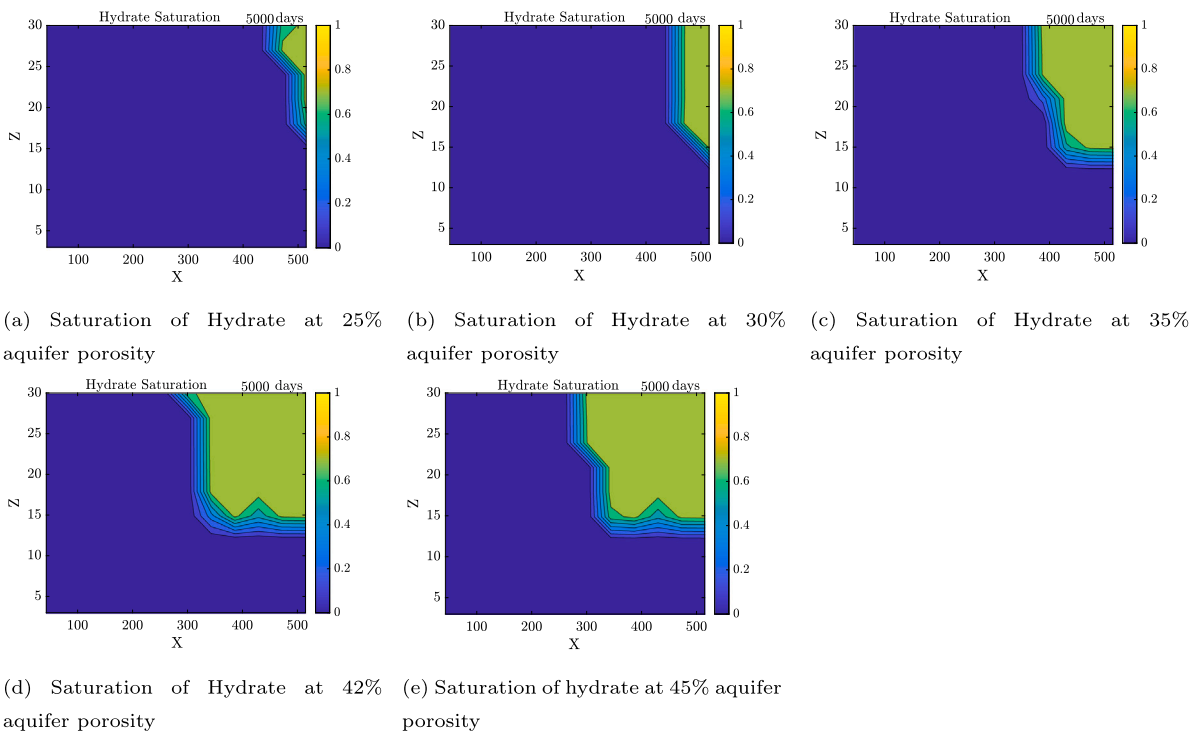
Fig. 10. Hydrate saturation profile at $5000\,days$ at various aquifer porosity and constant hydrate layer porosity of 42% when injector placed at the top.

Table 3
Well placement description in a layered hydrate zone.

Case	Injector location	Producer location	Pictorial representation
I_mid_P_top	At interface of HL1 and HL2	Near overburden	
I_top_P_top	At the top of HL1	Near overburden	
I_aquifer_P_top	Near aquifer	Near overburden	
Inj_P_mid	At interface of HL1 and HL2	At interface of HL1 and HL2	
I_top_P_mid	At the top of HL1	At interface of HL1 and HL2	
I_aquif_P_mid	Near aquifer	At interface of HL1 and HL2	
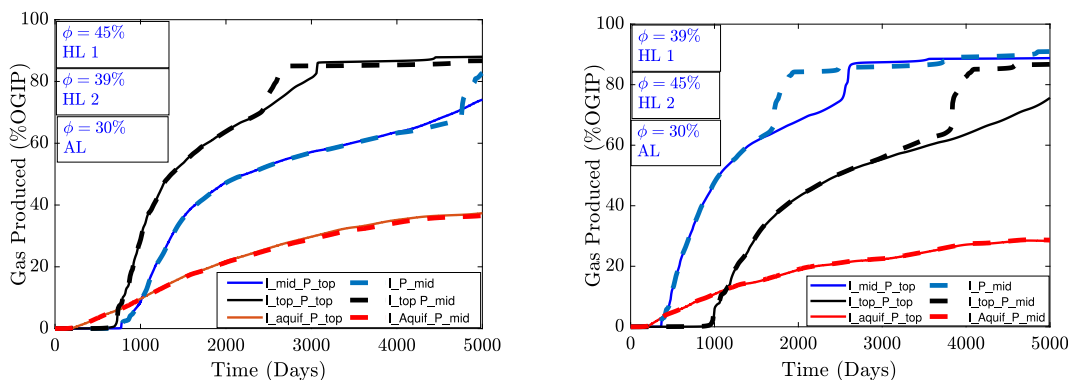
(a) Overall gas recovery (% OGIP) for different well locations at 30% aquifer porosity when hydrate layer near the overburden has HIGH porosity

(b) Overall gas recovery (% OGIP) for different well locations at 30% aquifer porosity when hydrate layer near the overburden has LOW porosity

Fig. 11. Gas recovery (% OGIP) for different well locations at 30% aquifer porosity when layers are introduced in hydrate zone.
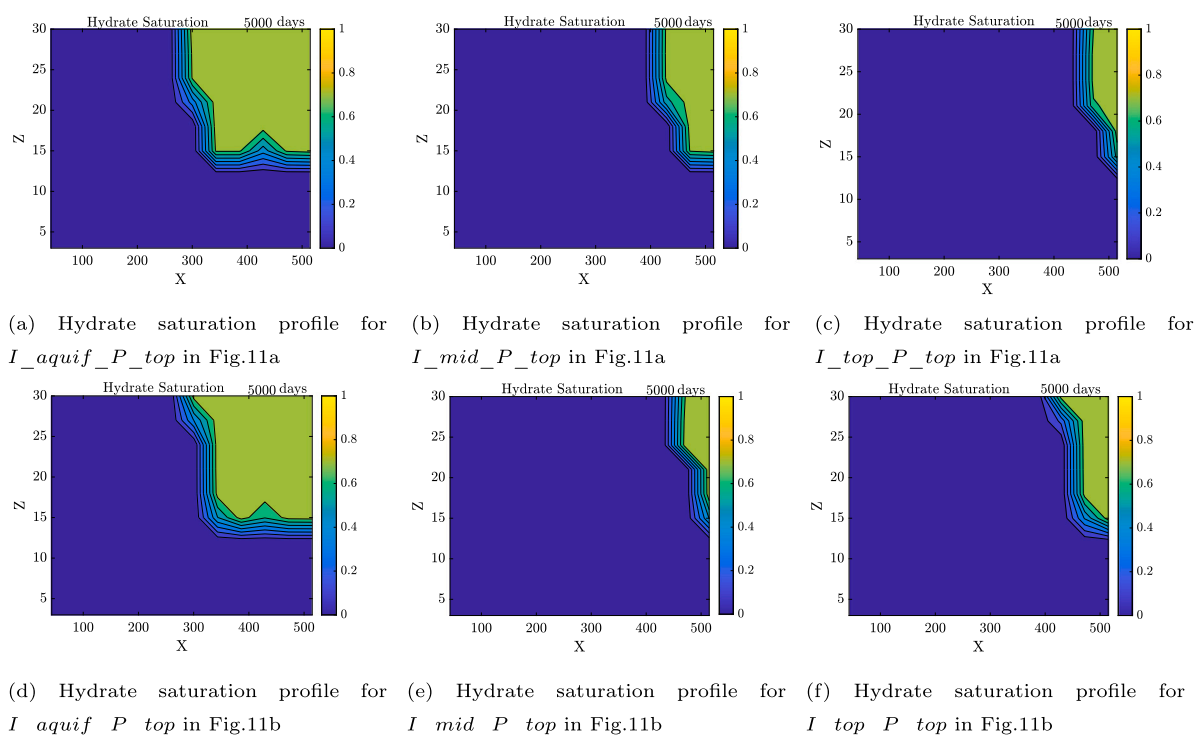
(a) Hydrate saturation profile for $I\_aquif\_P\_top$ in Fig.11a

(b) Hydrate saturation profile for $I\_mid\_P\_top$ in Fig.11a

(c) Hydrate saturation profile for $I\_top\_P\_top$ in Fig.11a

(d) Hydrate saturation profile for $I\_aquif\_P\_top$ in Fig.11b

(e) Hydrate saturation profile for $I\_mid\_P\_top$ in Fig.11b

(f) Hydrate saturation profile for $I\_top\_P\_top$ in Fig.11b

Fig. 12. Hydrate saturation profiles at $5000 days$ for different well locations when layers are introduced in hydrate zone.

However, the producer location does not have much effect on gas recovery. This is because, even for the moderate confinement of the reservoir, the depressurization is ineffective and most of the production is because of the warm water injection. Now, when the injector is placed near the aquifer, the energy of the injected warm water is wasted in the unconfined aquifer. However, when the injector is in the hydrate zone we see 65–85% recovery of the gas. When the production of different cases in Figs. 11(a) and 11(b) were compared, we see more production when the injector is in the high porosity layer in the hydrate zone. Therefore, in the layered, moderately unconfined, class-2 hydrate reservoirs the warm water should be injected in the high permeability hydrate layer. Hydrate saturation profiles in Fig. 12 also show higher gas recovery when the injector is placed away from the aquifer in a moderately unconfined reservoir.

Further, the effect of layering on the gas recovery in a hydrate reservoir attached to a highly unconfined aquifer was investigated.

Insets of Fig. 13 show porosity distribution in layers and Table 3 can be used to interpret the legends in the gas recovery curves. This study investigates two different locations of warm water injection: at the top of the hydrate layer and near the aquifer layer. Both the cases in Fig. 13 show that the injector location does not significantly impact the overall gas production, however, the injector in the hydrate zone delays the hydrate dissociation initially which was also reported in our previous work (Choudhary and Phirani, 2022).

4. Conclusion

The gas hydrate reservoirs found in nature are inherently heterogeneous and layered. This study examines the impact of layering on the class-2, unconfined hydrate reservoirs, similar to the reservoirs found in the Krishna–Godavary basin in India at site NGHP-02-09 (Collett et al., 2019). Warm water injection was used as the production method for these reservoirs. The results conclude that
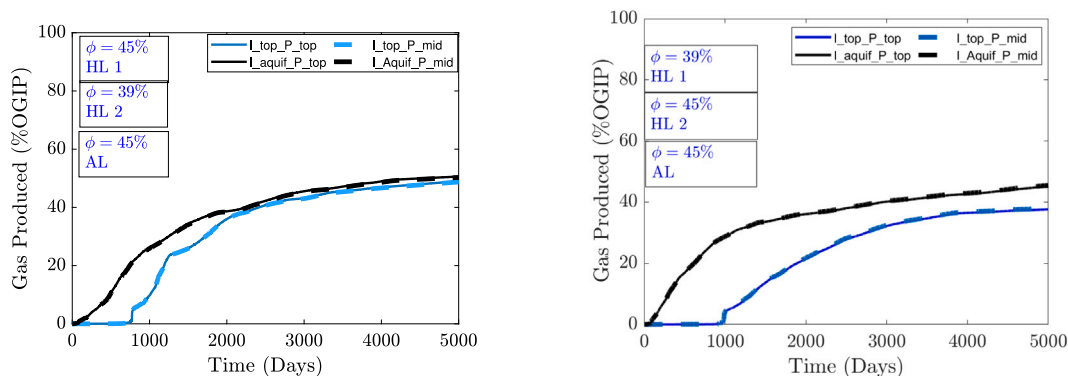
(a) Overall gas recovery (% OGIP) for different well locations at 45% aquifer porosity when hydrate layer near the overburden has HIGHER porosity

(b) Overall gas recovery (% OGIP) for different well locations at 45% aquifer porosity when hydrate layer near the overburden has LOW porosity

Fig. 13. Gas recovery (% OGIP) for different well locations at 45% aquifer porosity when layers are introduced in hydrate zone.

- The higher porosity of the aquifer leads to higher gas recovery in unconfined, class-2 hydrate reservoirs. This is because the warm water mobility increases with the increase in porosity and the permeability of the aquifer.
- In highly unconfined reservoirs, the injector should be placed in the proximity of the aquifer for better mobility of injected water.
- In moderately unconfined reservoirs, where water mobility is also limited in the aquifer, injector in the hydrate layer leads to more gas recovery.
- The layers in the hydrate zone in a highly unconfined reservoir do not significantly impact the overall gas recovery. However, in a moderately unconfined reservoir, the injector location in a high porosity hydrate layer leads to more gas recovery.

This study shows that characterizing the aquifer below the hydrate layer in class-2 hydrate reservoirs is very important. Injector location in these reservoirs will depend on the confinement of the aquifer below to improve the gas recovery.

CRediT authorship contribution statement

Neelam Choudhary: Investigation, Data curation, Writing – original draft, Software, Visualization, Formal analysis. **Jyoti Phirani:** Conceptualization, Methodology, Supervision, Writing – review & editing, Funding acquisition, Project administration, Resources, Formal analysis.

Data availability

No data was used for the research described in the article.

Acknowledgements

Declaration of competing interest

The authors declare that they have no known competing financial interests or personal relationships that could have appeared to influence the work reported in this paper.

References

Agency for Natural Resources and Energy (ANRE) and Japan Oil, Gas and Metals National Corporation (JOGMEC), 2017. Second offshore methane hydrate production test finishes. https://www.meti.go.jp/english/press/2017/0629_001.html. (Accessed 29 June 2017).

Aminnaji, M., Tohidi, B., Burgass, R., Atilhan, M., 2017. Gas hydrate blockage removal using chemical injection in vertical pipes. J. Nat. Gas Sci. Eng. 40, 17–23.

Bhade, P., Phirani, J., 2015a. Effect of geological layers on hydrate dissociation in natural gas hydrate reservoirs. J. Nat. Gas Sci. Eng. 26, 1549–1560.

Bhade, P., Phirani, J., 2015b. Gas production from layered methane hydrate reservoirs. Energy 82, 686–696.

Bhatnagar, G., Chapman, W.G., Dickens, G.R., Dugan, B., Hirasaki, G.J., 2006. Scaling of thermodynamic and transport processes for predicting methane hydrate saturation in marine sediments worldwide. In: SPE Annual Technical Conference and Exhibition. OnePetro.

Boswell, R., Myshakin, E., Moridis, G., Konno, Y., Collett, T.S., Reagan, M., Ajayi, T., Seol, Y., 2019. India National Gas Hydrate Program Expedition 02 summary of scientific results: Numerical simulation of reservoir response to depressurization. Mar. Pet. Geol. 108, 154–166.

Brooks, R., Corey, T., 1964. HYDRAU uc properties of porous media. Hydrol. Pap. Colorado State Univ. 24, 37.

Choudhary, N., Phirani, J., 2022. Effect of well configuration, well placement and reservoir characteristics on the performance of marine gas hydrate reservoir. Fuel 310, 122377.

Civan, F., 2001. Scale effect on porosity and permeability: Kinetics, model, and correlation. AIChE J. 47 (2), 271–287.

Civan, F., et al., 2002a. Fractal formulation of the porosity and permeability relationship resulting in a power-law flow units equation-a leaky-tube model. In: International Symposium and Exhibition on Formation Damage Control. Society of Petroleum Engineers.

Civan, F., et al., 2002b. Relating permeability to pore connectivity using a power-law flow unit equation. Petrophysics 43 (06).

Collett, T.S., Boswell, R., Waite, W.F., Kumar, P., Roy, S.K., Chopra, K., Singh, S.K., Yamada, Y., Tenma, N., Pohlman, J., et al., 2019. India National Gas Hydrate Program Expedition 02 summary of scientific results: gas hydrate systems along the eastern continental margin of India. Mar. Pet. Geol. 108, 39–142.

Dai, S., Santamarina, J.C., Waite, W.F., Kneafsey, T.J., 2012. Hydrate morphology: Physical properties of sands with patchy hydrate saturation. J. Geophys. Res. Solid Earth 117 (B11).

Falta, R.W., Pruess, K., Javandel, I., Witherspoon, P.A., 1992. Numerical modeling of steam injection for the removal of nonaqueous phase liquids from the subsurface: 1. Numerical formulation. Water Resour. Res. 28 (2), 433–449.

Feng, Y., Chen, L., Suzuki, A., Kogawa, T., Okajima, J., Komiya, A., Maruyama, S., 2019. Numerical analysis of gas production from layered methane hydrate reservoirs by depressurization. Energy 166, 1106–1119.

Graue, A., Kvamme, B., Baldwin, B.A., Stevens, J., Howard, J.J., Ersland, G., Husebo, J., Zornes, D.R., et al., 2006. Magnetic resonance imaging of methane-carbon dioxide hydrate reactions in sandstone pores. In: SPE Annual Technical Conference and Exhibition. Society of Petroleum Engineers.

Hao, Z., Fei, H., Hao, Q., Liu, L., 2017. China has successfully conducted its first pilot production of natural gas hydrates. Acta Geol. Sin. 91 (3), 1133–1134.

Hesselbo, S.P., Gröcke, D.R., Jenkyns, H.C., Bjerrum, C.J., Farrimond, P., Bell, H.S.M., Green, O.R., 2000. Massive dissociation of gas hydrate during a Jurassic oceanic anoxic event. Nature 406 (6794), 392.

Jang, J., Waite, W.F., Stern, L.A., Collett, T.S., Kumar, P., 2019. Physical property characteristics of gas hydrate-bearing reservoir and associated seal sediments collected during NGHP-02 in the Krishna-Godavari Basin, in the offshore of India. Mar. Pet. Geol. 108, 249–271.

Kakaee, A.-H., Paykani, A., 2013. Research and development of natural-gas fueled engines in Iran. Renew. Sustain. Energy Rev. 26, 805–821.

Kamath, V.A., Godbole, S.P., et al., 1987. Evaluation of hot-brine stimulation technique for gas production from natural gas hydrates. J. Pet. Technol. 39 (11), 1–379.

Kida, M., Jin, Y., Yoneda, J., Oshima, M., Kato, A., Konno, Y., Nagao, J., Tenma, N., 2019. Crystallographic and geochemical properties of natural gas hydrates accumulated in the National Gas Hydrate Program Expedition 02 drilling sites in the Krishna-Godavari Basin off India. Mar. Pet. Geol. 108, 471–481.

Kim, H., Bishnoi, P.R., Heidemann, R.A., Rizvi, S.S., 1987. Kinetics of methane hydrate decomposition. Chem. Eng. Sci. 42 (7), 1645–1653.

Konno, Y., Masuda, Y., Hariguchi, Y., Kurihara, M., Ouchi, H., 2010. Key factors for depressurization-induced gas production from oceanic methane hydrates. Energy Fuels 24 (3), 1736–1744.

Kvenvolden, K.A., 1993. Gas hydrates—geological perspective and global change. Rev. Geophys. 31 (2), 173–187.

Kvenvolden, K.A., 1999. Potential effects of gas hydrate on human welfare. Proc. Natl. Acad. Sci. 96 (7), 3420–3426.

Li, B., Liang, Y.-P., Li, X.-S., Zhou, L., 2016. A pilot-scale study of gas production from hydrate deposits with two-spot horizontal well system. Appl. Energy 176, 12–21.

Li, G., Wu, D., Li, X., Zhang, Y., Lv, Q., Wang, Y., 2017. Experimental investigation into the production behavior of methane hydrate under methanol injection in quartz sand. Energy Fuels 31 (5), 5411–5418.

Li, B., Zhang, T.-T., Wan, Q.-C., Feng, J.-C., Chen, L.-L., Wei, W.-N., 2021. Kinetic study of methane hydrate development involving the role of self-preservation effect in frozen sandy sediments. Appl. Energy 300, 117398.

Liu, J.-W., Li, X.-S., 2021. Recent advances on natural gas hydrate exploration and development in the South China Sea. Energy Fuels 35 (9), 7528–7552.

Luo, Y., Peng, J., Li, P., He, J., Li, L., 2015. Influence of heterogeneous hydrate distribution on the compressional wave velocity of hydrate-bearing sediment specimens. J. Nat. Gas Sci. Eng. 22, 90–97.

Makogon, Y.F., 2010. Natural gas hydrates–a promising source of energy. J. Nat. Gas Sci. Eng. 2 (1), 49–59.

Makogon, I.F., Makogon, I.F., Makogon, Y.F., 1997. Hydrates of Hydrocarbons. Pennwell Books.

Matsumoto, R., 2002. Comparison of marine and permafrost gas hydrates: Examples from Nankai Trough and Mackenzie Delta. In: Proc. 4th ICGH, 2002. pp. 1–6.

Matsuzawa, M., Terao, Y., Hay, B., Wingstrom, L., Duncan, M., Ayling, I., 2014. A completion system application for the world's first marine hydrate production test. In: Offshore Technology Conference. OnePetro.

Milkov, A.V., 2004. Global estimates of hydrate-bound gas in marine sediments: how much is really out there? Earth-Sci. Rev. 66 (3–4), 183–197.

Milkov, A.V., Sassen, R., 2001. Estimate of gas hydrate resource, northwestern Gulf of Mexico continental slope. Mar. Geol. 179 (1–2), 71–83.

Mohebbi, V., Behbahani, R., 2014. Experimental study on gas hydrate formation from natural gas mixture. J. Nat. Gas Sci. Eng. 18, 47–52.

Moridis, G.J., Kowalsky, M.B., Pruess, K., 2007. Depressurization-induced gas production from class-1 hydrate deposits. SPE Reserv. Eval. Eng. 10 (05), 458–481.

Myshakin, E.M., Gaddipati, M., Rose, K., Anderson, B.J., 2012. Numerical simulations of depressurization-induced gas production from gas hydrate reservoirs at the Walker Ridge 313 site, northern Gulf of Mexico. Mar. Pet. Geol. 34 (1), 169–185.

Phirani, J., Mohanty, K., 2009. Warm water flooding of confined gas hydrate reservoirs. Chem. Eng. Sci. 64 (10), 2361–2369.

Phirani, J., Mohanty, K.K., Hirasaki, G.J., 2009a. Warm water flooding of unconfined gas hydrate reservoirs. Energy Fuels 23 (9), 4507–4514.

Phirani, J., Mohanty, K.K., et al., 2010. Kinetic Simulation of CO_2 Flooding of methane hydrates. In: SPE Annual Technical Conference and Exhibition. Society of Petroleum Engineers.

Phirani, J., Pitchumani, R., Mohanty, K.K., et al., 2009b. History matching of hydrate formation and dissociation experiments in porous media. In: SPE Reservoir Simulation Symposium. Society of Petroleum Engineers.

Reagan, M.T., Moridis, G.J., Johnson, J.N., Pan, L., Freeman, C.M., Boyle, K.L., Keen, N.D., Husebo, J., 2015. Field-scale simulation of production from oceanic gas hydrate deposits. Transp. Porous Media 108 (1), 151–169.

Sira, J., Patil, S., Kamath, V., et al., 1990. Study of hydrate dissociation by methanol and glycol injection. In: SPE Annual Technical Conference and Exhibition. Society of Petroleum Engineers.

Sloan, Jr., E.D., 1998. Clathrate Hydrates of Natural Gases, Revised and Expanded. CRC Press.

Sun, X., Mohanty, K.K., 2006. Kinetic simulation of methane hydrate formation and dissociation in porous media. Chem. Eng. Sci. 61 (11), 3476–3495.

Uddin, M., Wright, F., Dallimore, S., Coombe, D., 2014. Gas hydrate dissociations in Mallik hydrate bearing zones A, B, and C by depressurization: Effect of salinity and hydration number in hydrate dissociation. J. Nat. Gas Sci. Eng. 21, 40–63.

Wan, Q.-C., Si, H., Li, G., Feng, J.-C., Li, B., 2020. Heterogeneity properties of methane hydrate formation in a pilot-scale hydrate simulator. Appl. Energy 261, 114325.

Wilder, J.W., Moridis, G.J., Wilson, S.J., Kurihara, M., White, M.D., Masuda, Y., Anderson, B.J., Collett, T.S., Hunter, R.B., Narita, H., et al., 2008. An international effort to compare gas hydrate reservoir simulators. In: Proceedings of 6th International Conference on Gas Hydrates. ICGH 2008, Vancouver, Canada.

Yamamoto, K., Kanno, T., Wang, X.-X., Tamaki, M., Fujii, T., Chee, S.-S., Wang, X.-W., Pimenov, V., Shako, V., 2017. Thermal responses of a gas hydrate-bearing sediment to a depressurization operation. RSC Adv. 7 (10), 5554–5577.

Yamamoto, K., Terao, Y., Fujii, T., Ikawa, T., Seki, M., Matsuzawa, M., Kanno, T., et al., 2014. Operational overview of the first offshore production test of methane hydrates in the Eastern Nankai Trough. In: Offshore Technology Conference.

Yamamoto, K., Wang, X.-X., Tamaki, M., Suzuki, K., 2019. The second offshore production of methane hydrate in the Nankai Trough and gas production behavior from a heterogeneous methane hydrate reservoir. RSC Adv. 9 (45), 25987–26013.

Yuan, Y., Xu, T., Xia, Y., Xin, X., 2018. Evaluation of gas productivity from layered heterogeneity methane hydrate reservoirs by depressurisation. In: Offshore Technology Conference Asia. OnePetro.

Yuan, Y., Xu, T., Xin, X., Xia, Y., 2017. Multiphase flow behavior of layered methane hydrate reservoir induced by gas production. Geofluids 2017.

Zhao, J., Zhu, Z., Song, Y., Liu, W., Zhang, Y., Wang, D., 2015. Analyzing the process of gas production for natural gas hydrate using depressurization. Appl. Energy 142, 125–134.